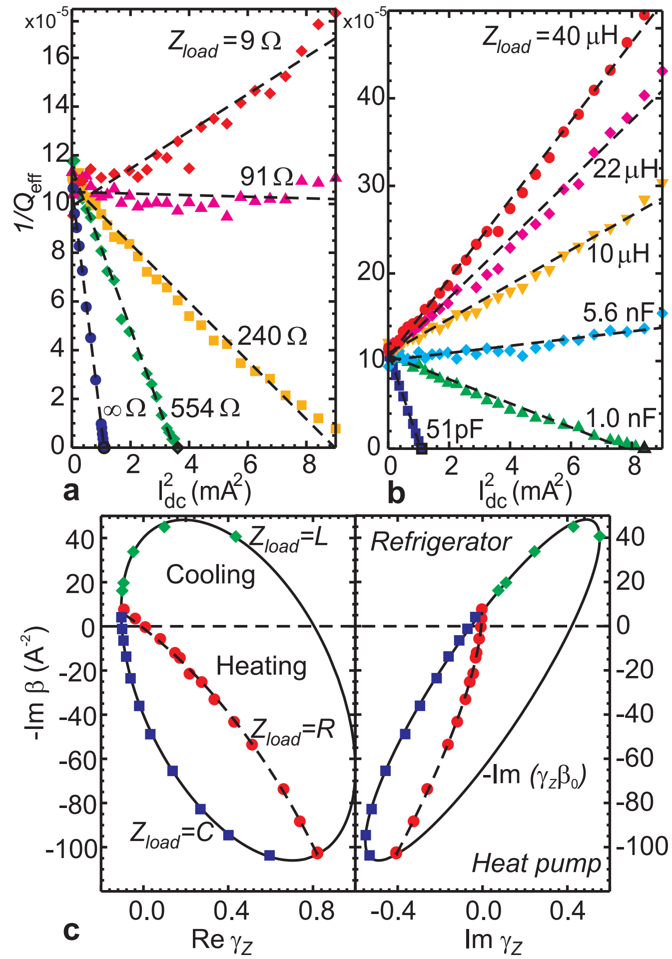

FIG. 4: **Measurements and fits to confirm the operation mechanism proposed in Fig. 1d. a,b** Inverse effective Q-factor $1/Q_{\rm eff}$ versus DC current I_{dc}^2 for different values of the load impedances $Z_{\rm load}$ indicated in the graph. Dashed lines are fits using equation (2). Symbols on the x-axis correspond to the minimum current level at which self-sustained oscillation was observed. **a** Resistive load impedances $Z_{\rm load}$. **b** Capacitive and inductive load impedances $Z_{\rm load}$. **c** Measured slopes $-{\rm Im}\ \beta$ of the curves in Fig. **a**,**b** plotted along the real (left) and the imaginary (right) γ_Z-axis for resistive (red circle), capacitive (blue square) and inductive (green diamond) values of $Z_{\rm load}$. An excellent fit of the data is obtained by plotting $-{\rm Im}\ (\gamma_Z\beta_0)$ with β_0=$-123.7+64.6iA^{-2}$, for resistive (dashed lines), capacitive and inductive (solid lines) values of $Z_{\rm load}$. If Im β is positive the engine beam acts as a heat pump that increases the effective temperature and if Im β is negative the engine beam acts as a refrigerator that cools the effective temperature of the resonance mode.

of these linear fits, Im β is determined and is plotted against γ_Z as symbols in Fig. 4c. As shown by solid and dashed lines in Fig. 4c, an excellent multiple linear regression fit of the data is obtained using the function Im β = Im $(\gamma_Z\beta_0)$, which yields the fit parameters $\beta_0 = -123.7 + 64.6i$ A^{-2} and $R_{beam} = 439.3\ \Omega$.

In Supplementary Discussion A an analytical model is derived for the complex Young's modulus and spring constant $k^*_{\rm eff}$ and it is used to derive an estimate for β_0, which yields $\beta_0 = -132 + 157i$ A^{-2}. A finite element simulation of the full geometry including the anisotropy of the silicon crystal results in $\beta_0 = -111+58i$ A^{-2}. Both the excellent fits in Fig. 3 and 4, and the quantitative agreement between the measured and simulated values of β_0 support the proposed feedback mechanism in Fig. 1d.

Flow rates of heat and work

In order to gain insight in the operation of the heat engine, a schematic showing the rate equations for the flow of heat and work between electrical source, heat sink, engine beam and resonance mode is shown in Fig. 5a. All rates shown in this figure are time averaged, such that all variations which cancel each other during a single cycle are averaged out. The three modes of operation which were experimentally observed in Fig. 2d, 3a, and 3b are shown in Fig. 5b. For Im $\beta < 0$, $\dot{W}_{he}$ is negative, thus cooling the effective temperature of the resonance mode and operating as a refrigerator. For $0 < Q_{\rm int} I_{dc}^2 {\rm Im}\beta < 1$ heat is pumped into the resonance mode, increasing $T_{\rm eff}$ until a new steady state is reached at which $\dot{W}_e + \dot{U}_i = 0$. In this mode the engine beam operates as a heat pump.